Invited paper

Sang-Eun Mun, Chulsoo Choi, Jongwoo Hong and Byoungho Lee*

Broadband wavelength demultiplexer using Fano-resonant metasurface

https://doi.org/10.1515/nanoph-2019-0492
Received November 30, 2019; revised January 1, 2020; accepted January 4, 2020

Abstract: Fano resonance, one of the interesting resonance phenomena in physics, provides versatile applications when combined with a concept of metasurface in nanophotonics. Fano-resonant metasurface (FRM) is attracting a lot of attention due to its superior narrowband characteristics as well as design freedom of metasurfaces in nanoscale. However, only the control of apparent asymmetric spectral nature of Fano resonance has been focused at applications such as optical sensors, as the amplitude feature of Fano resonances is relatively easy to control and can be measured by an experimental setup. Here, a method for modulating the phase information of FRM by both simulation and experiment is demonstrated. As a proof of concept, an optical demultiplexer, which can divide four target wavelengths in different directions of free space, is verified experimentally. It covers a broadband wavelength range of more than 350 nm in the near-infrared region with extremely small full-width at half-maximum. This approach can offer the complete control of FRM for a wide range of applications, including optical multiplexers, routers, filters, and switches, beyond conventional applications that have been limited to the amplitude control of Fano resonance.

Keywords: Fano resonance; metasurface; optical demultiplexer; wavelength selective; beam deflection.

***Corresponding author: Byoungho Lee,** School of Electrical and Computer Engineering and Inter-University Semiconductor Research Center, Seoul National University, Gwanak-Gu Gwanakro 1, Seoul 08826, Republic of Korea, e-mail: byoungho@snu.ac.kr. https://orcid.org/0000-0002-0477-9539
Sang-Eun Mun, Chulsoo Choi and Jongwoo Hong: School of Electrical and Computer Engineering and Inter-University Semiconductor Research Center, Seoul National University, Gwanak-Gu Gwanakro 1, Seoul 08826, Republic of Korea

1 Introduction

Fano resonance is a resonant phenomenon originating from the destructive interference between superradiant and subradiant modes in quantum physics, which was first proposed by Ugo Fano in 1935 [1]. The unique feature of Fano resonance, a distinctly asymmetric line shape in far-field spectrum, is the large number of potential applications in the development of nanophotonics as well as atomic systems [2–5]. In recent decades, metasurfaces that are composed of arbitrarily designed sub-wavelength-scale antennas have been widely researched due to their outstanding characteristics for light modulation within a small footprint [6–13]. They have also been spotlighted as a platform for inducing and manipulating Fano resonance [8–13]. The excitation of Fano resonance has been demonstrated by various types of nanostructures such as split-ring resonators [9], asymmetric double bars [10, 11], hybrid nanoparticles [12], and dolmen structure [13]. Especially, thanks to its characteristic that exhibits the high-quality factor within narrowband spectrum, Fano-resonant metasurfaces (FRMs) have been applied to various optical devices, including ultrasensitive spectroscopy [14], chemical sensing or biosensing [15–17], and optical logic operation [18].

To further improve the prominent advantages of Fano resonance, such as high-quality factor and asymmetric line shape in the amplitude spectrum, numerous studies have focused on using and modulating these factors. FRMs have been proposed that enhance the quality factor [19–22], tune the resonance frequencies [23, 24], control the modulation depth [25, 26], and excite multiple resonances [16, 27, 28] by changing geometric parameters. Very recently, the active mechanism is implemented to extend the functionality of FRMs [29–32]. This research flow has only established limited applications using the amplitude and intensity characteristics of Fano resonance. In addition to this intuitive approach, Fano resonances can be applied in a wider range using phase or polarization nature with narrow bandwidth. However, despite many other possibilities for optical elements, studies using other optical characteristics of Fano resonance have been elusive.

In the condition of Fano resonance excitation, a unique phase jump is a notable phenomenon, which appears near Fano resonance wavelength depending on the relative quantitative conditions of the radiative loss and coupling coefficient [2]. In terms of wavelength-selective applications, such as optical routing and optical demultiplexing, FRM can be a superior candidate using phase modulation property. Recently, a color routing based on FRM is demonstrated as one of the few examples using phase modulation of Fano resonance [33]. However, there has been no demonstration about optical demultiplexers through FRM, although it has a great potential to improve the functionality dramatically. Until now, optical demultiplexers implemented in nanophotonics have limited platforms such as waveguide, cavity, and in-plane propagating structures [34–36]. They also have limitations, such as fewer target wavelengths, narrow operating range, high crosstalk, and large full-width at half-maximum (FWHM) of the target wavelength. These problems can be improved using the narrowband characteristics of Fano resonance.

In this paper, a phase modulation mechanism of Fano resonance is introduced. Distinct from conventional approaches that control a spectral line shape of Fano resonance, a new scheme of Fano-based optical device is proposed by adjusting a phase jump characteristic through ultra-thin metasurface. The proposed metasurface, composed of gold nanorods on a gold backplane film with dielectric spacer between them, supports multiple Fano resonances as well as dipolar resonance, which can deflect only the specific wavelength corresponding to the condition of Fano resonance without distortion between the other target wavelengths. Hence, a function of optical demultiplexer is implemented by multiplexing the gradient metasurface in a wide near-infrared (IR) spectral range.

2 Results and Discussion

2.1 Operating principle of phase modulation in FRM

A schematic of the proposed metasurface consists of three layers: a ground gold plane, a dielectric spacer, and a top layer of triple gold nanorods (Figure 1A). Each layer has a thickness of 100, 80, and 50 nm from the bottom, respectively. The unit cell consists of triple gold nanorods with different lengths to support multiple Fano resonances, and the unit structure is arranged in a period of 650 nm in both x and y directions ($P_x = P_y$). The lengths of gold nanorods are denoted as L_1, L_2, and L_3, respectively. L_1 is fixed as 420 nm and the others would be controlled to induce Fano resonance independently. All nanorods have

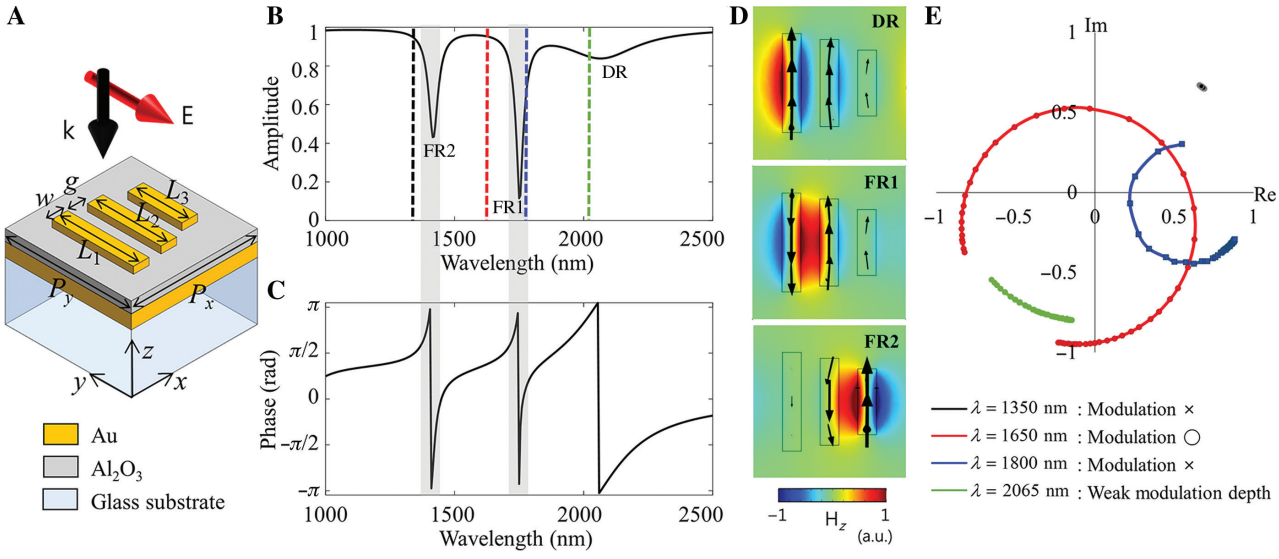

Figure 1: Proposed metasurface and its numerical analysis.
(A) Schematic illustration of FRM in reflection form composed of triple gold nanorods with dielectric spacer above the gold film. Incident light has a y-polarized electric field. Amplitude (B) and phase (C) of the reflected light for the proposed metasurface. DR, FR1, and FR2 indicate the dipole, first Fano, and second Fano resonances in sequence. Gray shaded areas represent phase modulation at Fano resonances. Dashed color lines indicate the wavelengths to be used for analysis in (E). (D) Magnetic field distribution in z direction for each resonance condition with black arrows of induced current density. (E) Modulation characteristics for each wavelength near the DR, FR1, and FR2 regions in the complex plane when the nanorod length changes.

width (w) of 80 nm and gap (g) of 80 nm between each rod. For numerical verification, a commercial simulation tool (COMSOL Multiphysics 5.3) is employed.

To make plasmonic resonances on metallic nanorods, a y-polarized electric field is normally incident from the upper side of the metasurface. When the proper condition of lengths (L_2 = 370 nm and L_3 = 280 nm) is established, the amplitude and phase spectra of the reflected light are shown in Figure 1B and C. Among the observed three resonance modes, a dipole resonance (DR) in which the current densities are induced in the same directions for all three nanorods appears at the longest wavelength. The first Fano resonance (FR1) and the second Fano resonance (FR2) are distinct spectral features manifested by different Fano resonance modes. The out-of-phase current density excitation in two longer pairs of the three nanorods is referred to as FR1 and that in the shorter pairs is FR2. The magnetic field distributions in z direction for each mode are shown in Figure 1D with the induced current density of black arrows. These amplitude characteristics are due to the coupling of the circulating currents induced between the ground gold film and nanorods, as reported previously [19].

Herein, the focus is on the phase shift phenomenon at each resonance wavelength as shown in Figure 1C. When the designed metasurface is composed of a reflection scheme, the total reflected light can be expressed as follows:

$$R = r_{12} + t_{12} e^{i(\pi + 4\pi nd/\lambda)} \cdot \frac{1}{1 - r_{21} e^{i(\pi + 4\pi nd/\lambda)}} \cdot t_{21}, \quad (1)$$

where r_{12} and t_{12} are the reflection and transmission coefficients from layer 1 to layer 2 and r_{21} and t_{21} are those from layer 2 to layer 1, respectively. The parameter λ is the wavelength of light in free space, n is the refractive index of the dielectric spacer, and d is the thickness of the dielectric spacer causing the Fabry-Pérot cavity effect. The reflection and transmission coefficients can be substituted by normalizing the eigenvectors when modeled with a coupled harmonic oscillator system. When the phase information of the total reflected light is examined by appropriately sweeping the coupling parameter, it is found that a dramatic phase change of about 2π appears near the wavelength where Fano resonance occurs. It can be inferred that full phase modulation is possible in the reflective structure, unlike a π phase jump in a single-layer FRM. To intuitively represent only the phase modulation caused by the resonant structure, Figure 1C shows the phase information subtracting the phase occurred by light propagation. Although a full phase modulation occurs even in a simple perfect absorber-like structure with a bottom metal film [37], there is a difference that the full phase modulation based on FRM has exceptional wavelength-selective characteristics. The detailed conditions are described in the Supplementary Information.

Numerical results are analyzed to verify the theoretical prediction. Figure 1E shows an example of the modulation characteristics based on Fano resonance in the complex plane that occurs when the length conditions of L_2 and L_3 change. For example, if the FR1 mode is targeted, the lengths of L_1 and L_3 are fixed as 420 and 280 nm, respectively. The modulation pattern observed near the wavelength of each resonance condition is different as the length of L_2 varies from 390 to 300 nm. First, when the oscillating electrons in all nanorods are in phase (DR condition), the wavelength condition of the localized surface plasmon resonance shifts slightly as the L_2 changes, resulting in a phase modulation with a very weak modulation depth (Figure 1E, green line). In contrast, as the length of L_3 is fixed, no phase modulation is found at a fixed wavelength near the FR2 no matter how L_2 changes (Figure 1E, black line). In the case of FR1 to be targeted, the phase jump occurs in the region longer than Fano resonance wavelength but does not cover as much as 2π (Figure 1E, blue line). Thus, if the wavelength is selected in a range slightly smaller than the Fano resonance wavelength (λ = 1650 nm in here), all four regions of the quadrant can be covered (Figure 1E, red line). Due to the high Q factor of Fano resonance, a much sharper modulation depth can be achieved than in the case of DR. If the FR2 mode is targeted, it is obvious that similar phenomena occur in the wavelength region near FR2. Therefore, selecting an appropriate target wavelength near Fano resonance is a design strategy that enables a full phase modulation in the narrow bandwidth. The proposed structure enables the phase control of two target wavelengths in one unit cell structure using multiple Fano resonances. Also, the thickness of dielectric spacer is optimized with 80 nm to minimize the amplitude fluctuation, which can be caused by the reflection dip of Fano resonance almost close to zero. Using the phase modulation characteristic of Fano resonance, the metasurface as an optical device will be proposed in the next section.

2.2 Gradient metasurface and optical demultiplexer

A gradient metasurface is demonstrated by arranging three unit cells of the multiple FRM discussed above. Each supercell targets two separate wavelengths based on the double Fano resonances, i.e. FR1 and FR2. If the phase step

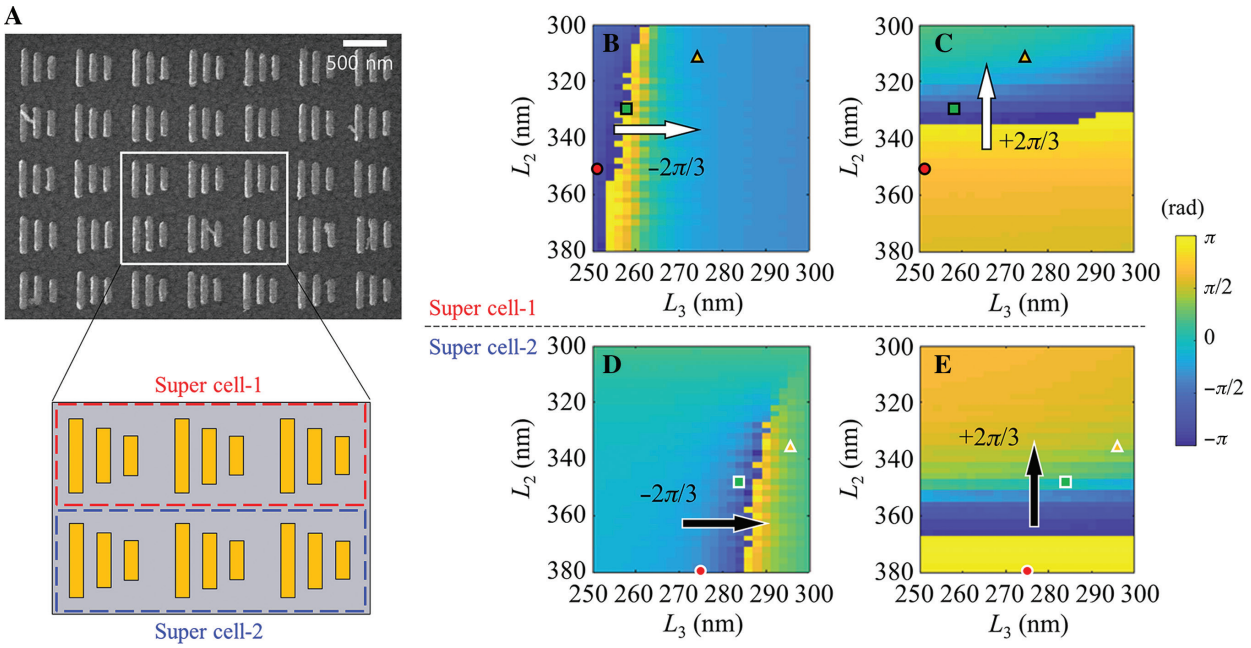

Figure 2: Design of gradient metasurface for optical demultiplexer.
(A) Schematic illustration of a gradient metasurface for the function of optical demultiplexer. (B–E) Numerically calculated phase values to design gradient metasurface according to the change of L_2 and L_3. Phase maps of target wavelengths (B) 1344 nm and (C) 1610 nm for supercell-1 and (D) 1440 nm and (E) 1700 nm for supercell-2. Each marker (circles, squares, and triangles) and an arrow indicate the selected geometric parameters of the length and gradient phase steps.

is set to a different sign at each resonance, the wavevector of the reflected light due to one supercell is expressed as

$$k_{\parallel}^{\text{out}} = k_{\parallel}^{\text{in}} + \frac{\partial \Phi(\lambda)}{\partial x} \begin{cases} \frac{\partial \Phi(\lambda_a)}{\partial x} = \frac{-2\pi}{\Lambda} \\ \frac{\partial \Phi(\lambda_{\text{else}})}{\partial x} = 0 \\ \frac{\partial \Phi(\lambda_b)}{\partial x} = \frac{2\pi}{\Lambda} \end{cases}, \quad (2)$$

where λ_a and λ_b are the target wavelengths of one supercell. The parameter Λ is equal to $3P_x$ in the entire period of the supercell. For the output wavevectors of target wavelengths λ_a and λ_b, the gradient values having a different sign are added in the x direction, and all other wavelengths, except the target wavelengths, are reflected in the incident direction. Then, the deflection angle of each target wavelength is given by

$$\theta = \pm \sin(\lambda/\Lambda). \quad (3)$$

In addition, the proposed device is composed of two supercells of gradient metasurfaces to expand the functionality of an optical demultiplexer that can separate multiple wavelengths into different channels as shown in Figure 2A. Each supercell targets two separate wavelengths. Figure 2B–E illustrates the phase map of the reflected light by the change of L_2 and L_3. The length condition shown in Figure 2A is designed based on the conditions marked with circles, squares, and triangles. Figure 2B and C represents the phase information for designing supercell-1 at the target wavelengths of 1344 and 1610 nm, respectively. Figure 2D and E shows the phase information for designing supercell-2 at the target wavelengths of 1440 and 1700 nm, respectively. It can be seen that there is a very sharp phase flip near the areas where Fano resonance occurs. In particular, it is important to note that Figure 2B and D exhibits phase variation according to the change of L_3, as it depends on FR2 basis. In contrast, phase variation in Figure 2C and E only depends on L_2 value regardless of L_3, as it is based on FR1. To achieve high angle deflection, each marker has a phase difference of magnitude $2\pi/3$ sequentially. As indicated by the arrow, the phase step is $-2\pi/3$ when the short wavelength is targeted in each supercell (for FR2) and $+2\pi/3$ for the target of the long wavelength (for FR1). Thus, the targeted short and long wavelengths are deflected in different directions. The final designed geometric parameters (L_1, L_2, L_3) are (420, 356, 250), (420, 328, 258), and (420, 312, 274) nm for supercell-1 and (420, 382, 274), (420, 348, 284), and (420, 336, 296) nm for supercell-2. The detailed information on the amplitude and phase of each unit cell is given in the Supplementary Information.

The scattered electric fields for each targeted wavelength are shown in Figure 3A. As designed above, it is confirmed that two short wavelengths (1344 and

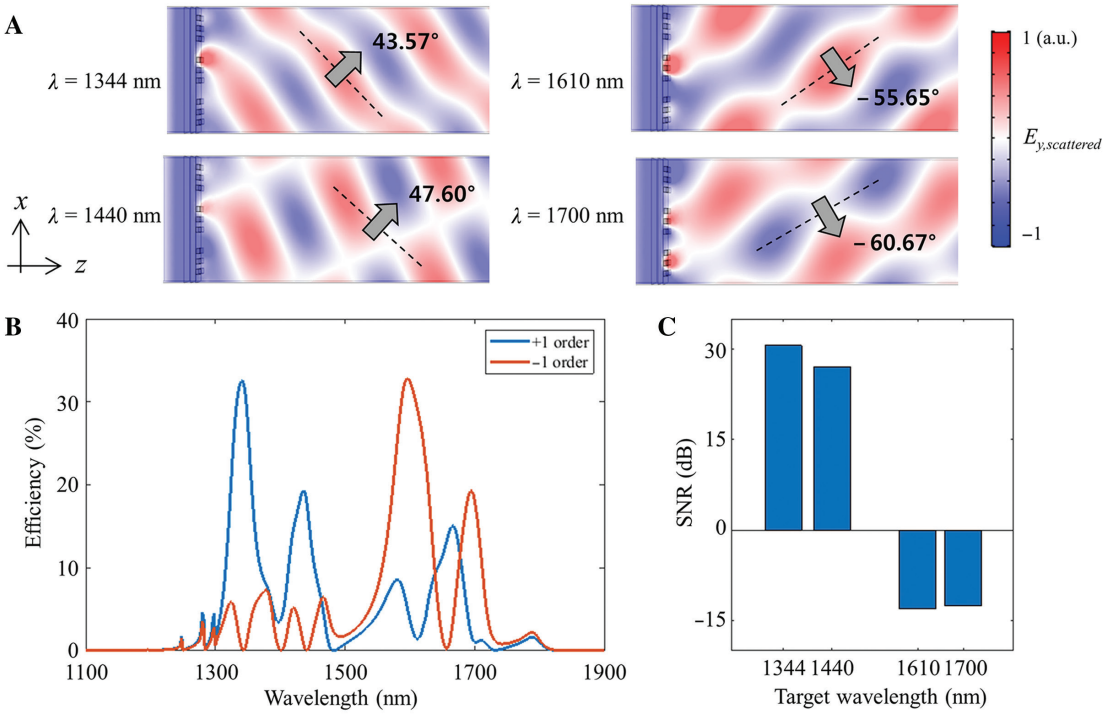

Figure 3: Numerical results for the performance of the proposed metasurface.
(A) Scattered electric field distributions (E_y) of reflected light for four target wavelengths 1344, 1440, 1610, and 1700 nm. Each arrow and dotted line indicate deflection direction and wavefront with angle information, respectively. (B) Diffraction efficiency for the + and - first-order directions in the case of broadband source illumination. (C) SNR at each target wavelength.

1440 nm) are deflected in the $+x$ direction and two long wavelengths (1610 and 1700 nm) are deflected in the $-x$ direction, respectively. The efficiency for each diffraction order and signal-to-noise ratio (SNR) for target order number are represented in Figure 3B and C. The efficiencies at target wavelength 1344, 1440, 1610, and 1700 nm are 32.55%, 19.36%, 32.82%, and 19.29% and the calculated FWHM are 38, 41, 61, and 37 nm, respectively. Each wavelength exhibits outstanding narrowband characteristics without crosstalk with each other, which is a superior advantage as an optical demultiplexer compared to the conventional studies based on the waveguide and cavity system [34–36]. The SNR is defined as the intensity ratio of the target order to the orthogonal one in dB scale, i.e. SNR = 10 log($I_\sigma/I_{\sigma'}$) [dB], where $(\sigma, \sigma') = (+1, -1)$. The absolute values of SNR for each wavelength are 30.59, 27.03, 13.05, and 12.59 dB, respectively. As inferred from Figure 1B, the FR2-based modulation target wavelength has a weaker antisymmetric mode coupling than FR1, resulting in higher and broader amplitude characteristics than FR1. That is why the efficiency and SNR in the short wavelengths 1344 and 1440 nm are higher than those of long wavelengths.

Figure 4 shows the experimental results for the demonstration of the proposed optical demultiplexer. The fabrication is carried out using conventional e-beam lithography process (see Materials and methods). The sample is fabricated with an overall area of 500×500 μm^2. The length of each nanorod on the fabricated sample is almost similar to the designed value. Although it has an error of less than 20 nm, it maintains the length disparity between each nanorod well (see Supplementary Information). Figure 4B and C shows the captured Fourier plane images and intensities of the reflected light, measured at a specific deflection angle position. The angles shown in Figure 4B are measured through the rotation stage on the measurement setup (see Supplementary Information). The average value of the measured deflection angles (45.3°, 50.5°, −57.8°, and −62.0°) is found to be in good agreement with the value designed by the simulation (43.57°, 47.60°, −55.65°, and −60.67°), which is confirmed in Figure 5A. The calculated angle deviation has an error up to 7.58° as shown in Figure 5B. The reason that the measured angle tends to be slightly larger than the designed value is related to a little longer fabricated rod length

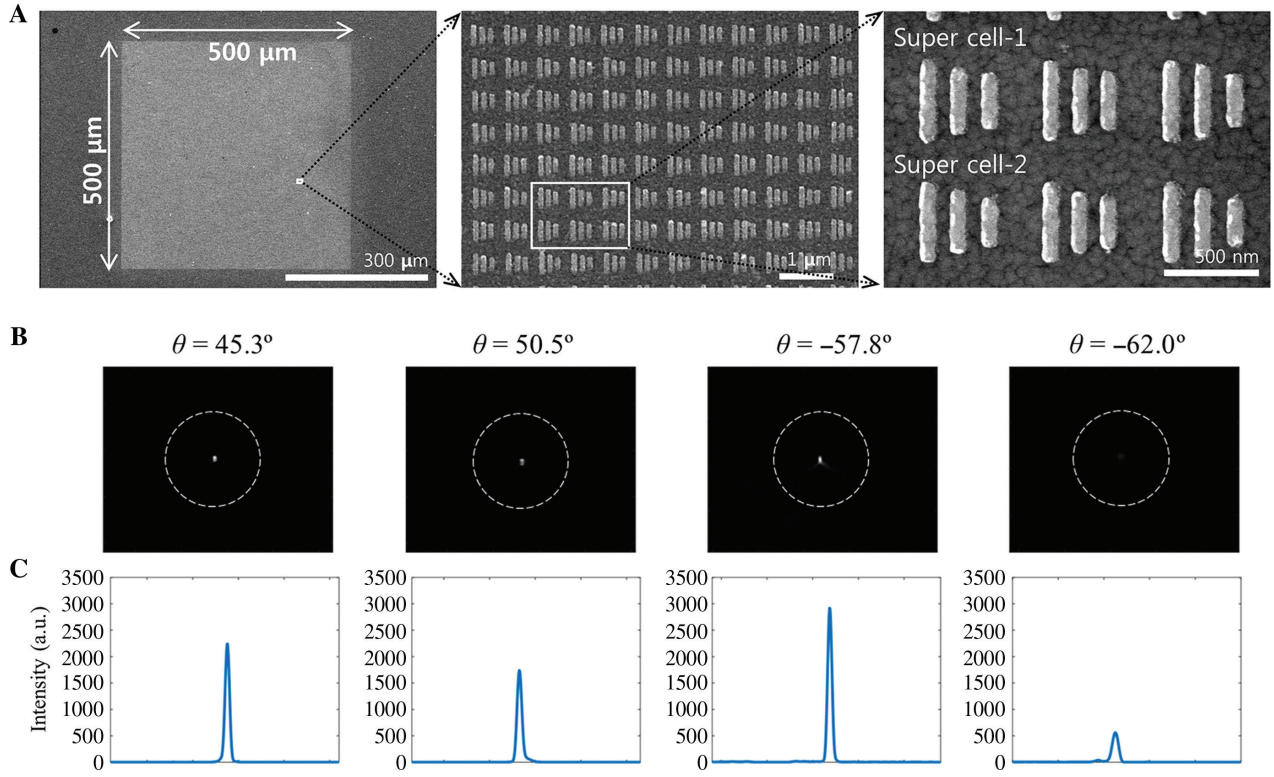

Figure 4: Fabricated metasurface and its experimental results.
(A) Field emission-scanning electron microscopy images of the fabricated metasurface samples at different magnifications. The total size of sample is 500×500 μm². (B) Captured CCD images on the Fourier plane for each target wavelength and the measured deflection angles at that time. (C) Intensity corresponding to the above CCD images, which is plotted on an arbitrary unit for efficiency comparison.

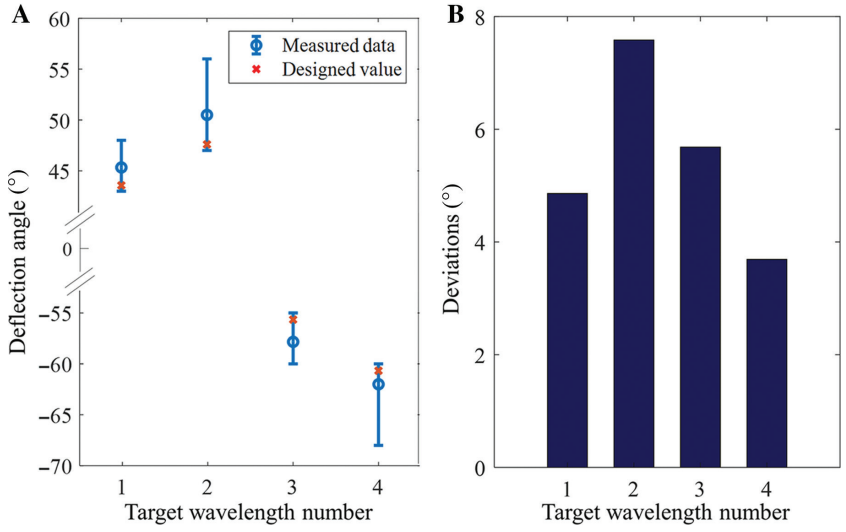

Figure 5: Measurement results.
(A) Measured deflection angles (blue circle marker) with error bar for four target wavelengths. Target wavelength numbers 1–4 represent the case of designed wavelengths 1344, 1400, 1610, and 1700 nm, respectively. Red cross markers indicate the deflection angles at each of the designed wavelengths. (B) Deviation of the measured angles for each target wavelength.

conditions and the spacer thickness optimization (see Supplementary Information). The dielectric thickness deposited by sputter equipment is slightly smaller than the target 80 nm, which leads to red shift in wavelength. The efficiency of each deflected light is calculated from Figure 4C with reference data, which is 5.75%, 4.46%, 7.49%, and 1.44%. Although the absolute value of efficiency has been considerably reduced overall, the

efficiency magnitude ratio at each wavelength is similar to the simulation results. By applying this measured angle to equation $\lambda = 3P_x \sin(\theta)$, wavelength information of the deflected light measured on each Fourier plane can be derived. The broadband source is used without a filter, which cannot properly filter out very narrowband target wavelengths, so measurements are made using this inverse calculation method. The wavelengths of the deflected light calculated from this equation are inferred as 1386, 1505, 1650, and 1722 nm, respectively, which can be considered to closely match the targeted values. Consequently, the ability of the optical demultiplexer is demonstrated to isolate the target wavelengths as designed, which makes sense by taking advantages of the extreme narrowband nature of Fano resonance.

3 Conclusion

In summary, a novel concept of phase modulation based on FRM was introduced and experimentally demonstrated. A broadband optical demultiplexer using FRM was proposed as one of the application examples in the near-IR spectral region. The reflective structure was numerically investigated to overcome the limitation of single-layer FRM that can provide only an abrupt π phase change and verify the possibility of full phase modulation. The reflection-type metasurface enabled the phase modulation from 0 to 2π in a very narrowband region near the wavelength where Fano resonance occurs. In addition, by inducing multiple Fano resonances using triple nanorod structure and spatial multiplexing technique, the proposed metasurface was capable of steering light to large deflection angles only for four target wavelengths without crosstalk. The proposed structure separated four target wavelengths by 45.3°, 50.5°, −57.8°, and −62.0°, respectively, and had a maximum SNR of 61.17 dB at 1344 nm wavelength. The proposed device displayed wide bandwidths (>350 nm) and extremely small FWHM (especially 37 nm at 1700 nm) with $500 \times 500\ \mu m^2$ small feature size. The proposed structure gives insight into multiple Fano resonances, so that the number of demultiplexing channels can be extended to four or more using more multiple Fano resonances. In addition, the perspective of a transmissive structure is expected based on the proposed theoretical analysis. The proposed scheme will explore the application of FRM, which is limited to conventional amplitude control thus far, and will be a new platform for various optical applications in narrowband as well as broadband operation ranges.

See Supplementary Information for the supporting content.

4 Materials and methods

The fabrication of FRM was performed using conventional e-beam lithography technique. First, chromium as an adhesion layer and gold mirror films with a thickness of 2 and 100 nm, respectively, were deposited via a thermal evaporator (MHS-1800) on a glass substrate. Then, aluminum oxide with 80 nm thickness was deposited by sputtering (SNTEK sputter, PSP5004). Bilayer e-beam resists (PMMA 495K A4 and 950K A2) were sequentially spin-coated on top of the sample after sputtering. The periodic array composed of triple gold nanorods was patterned with a high-resolution e-beam lithography technique (JBX-6300FS) operating at 100 kV condition. After development, a gold layer of 50 nm was deposited by a thermal evaporator. Finally, the patterned FRM was completed through a lift-off process.

To characterize the optical resonance of the sample, a broadband measurement setup was used with a CCD camera system. Broadband source (ANDO, AQ-4303B) covering the whole near-IR region (from 400 to 1800 nm) was used, and linear polarizer and lens for collimating the divergence of broadband light were used in front of the source. To avoid high k incident components, incident light was focused on the sample using a long focal length lens. The rotation stage was used to center the sample, and the Fourier plane was captured by an IR CCD camera (PAMINA) after passing the 4f system on the rotation stage rail. The light spot appearing on the Fourier plane was scanned with a CCD camera and the deflection angle was measured simultaneously.

Acknowledgments: The authors acknowledge the support from the Brain Korea 21 (BK21) project. This research was supported in part by Samsung Electronics.

Conflict of interest: The authors declare no conflict of interest.

References

[1] Fano U. Effects of configuration interaction on intensities and phase shifts. Phys Rev 1961;124:1866.
[2] Joe YS, Satanin AM, Kim CS. Classical analogy of Fano resonances. Phys Scr 2006;74:259.
[3] Luk'yanchuk B, Zheludev NI, Maier SA, et al. The Fano resonance in plasmonic nanostructures and metamaterials. Nat Mater 2010;9:707.
[4] Rahmani M, Luk'yanchuk1 B, Hong M. Fano resonance in novel plasmonic nanostructures. Laser Photon Rev 2013;7:329–49.
[5] Limonov MF, Rybin MV, Poddubny AN, Kivshar YS. Fano resonances in photonics. Nat Photonics 2017;11:543–54.

[6] Sung J, Lee G-Y, Lee B. Progresses in the practical metasurface for holography and lens. Nanophotonics 2019;8:1701–18.
[7] Choi C, Lee S-Y, Mun S-E, et al. Metasurface with nanostructured Ge2Sb2Te5 as a platform for broadband-operating wavefront switch. Adv Opt Mater 2019;7:1900171.
[8] Mun S-E, Lee K, Yun H, Lee B. Polarization-independent plasmon-induced transparency in a symmetric metamaterial. Adv Opt Mater 2016;28:2581–4.
[9] Fedotov VA, Rose M, Prosvirnin SL, Papasimakis N, Zheludev NI. Sharp trapped-mode resonances in planar metamaterials with a broken structural symmetry. Phys Rev Lett 2007;99:147401.
[10] Moritake Y, Kanamori Y, Hane K. Experimental demonstration of sharp Fano resonance in optical metamaterials composed of asymmetric double bars. Opt Lett 2014;39:4057–60.
[11] Dong Z-G, Liu H, Xu M-X, et al. Plasmonically induced transparent magnetic resonance in a metallic metamaterial composed of asymmetric double bars. Opt Express 2010;18:18229.
[12] Verellen N, Sonnefraud Y, Sobhani H, et al. Fano resonances in individual coherent plasmonic nanocavities. Nano Lett 2009;9:1663–7.
[13] Zhang S, Genov DA, Wang Y, Liu M, Zhang X. Plasmon-induced transparency in metamaterials. Phys Rev Lett 2008;101:047401.
[14] Wu C, Khanikaev AB, Adato R, et al. Fano-resonant asymmetric metamaterials for ultrasensitive spectroscopy and identification of molecular monolayers. Nat Mater 2012;11:69.
[15] Semouchkina E, Duan R, Semouchkin G, Pandey R. Sensing based on Fano-type resonance response of all-dielectric metamaterials. Sensors 2015;15:9344.
[16] Zhang Y, Liu W, Li Z, et al. High-quality-factor multiple Fano resonances for refractive index sensing. Opt Lett 2018;43:1842–5.
[17] Srivastava YK, Ako RT, Gupta M, Bhaskaran M, Sriram S, Singh R. Terahertz sensing of 7 nm dielectric film with bound states in the continuum metasurfaces. Appl Phys Lett 2019;115:151105.
[18] Manjappa M, Pitchappa P, Singh N, et al. Reconfigurable MEMS Fano metasurfaces with multiple-input-output states for logic operations at terahertz frequencies. Nat Commun 2018;9:4056.
[19] Mun S-E, Yun H, Choi C, Kim S-J, Lee B. Enhancement and switching of Fano resonance in metamaterial. Adv Opt Mater 2018;6:1800545.
[20] Yang Y, Kravchenko II, Briggs DP, Valentine J. All-dielectric metasurface analogue of electromagnetically induced transparency. Nat Commun 2014;5:5753.
[21] Cong L, Manjappa M, Xu N, Al-Naib I, Zhang W, Singh R. Fano resonances in terahertz metasurfaces: a figure of merit optimization. Adv Opt Mater 2015;3:1537.
[22] Moritake Y, Kanamori Y, Hane K. Enhanced quality factor of Fano resonance in optical metamaterials by manipulating configuration of unit cells. Appl Phys Lett 2015;107:211108.
[23] Cao T, Wei C, Simpson RE, Zhang L, Cryan MJ. Fast tuning of Fano resonance in metal/phase-change materials/metal metamaterials. Opt Mater Express 2014;4:1775–86.
[24] Deng Z-L, Yogesh N, Chen X-D, et al. Full controlling of Fano resonances in metal-slit superlattice. Sci Rep 2015;5:18461.
[25] Lassiter JB, Sobhani H, Knight MW, Mielczarek WS, Nordlander P, Halas NJ. Designing and deconstructing the Fano lineshape in plasmonic nanoclusters. Nano Lett 2012;12:1058–62.
[26] Emani NK, Chung T-F, Kildishev AV, Shalaev VM, Chen YP, Boltasseva A. Electrical modulation of Fano resonance in plasmonic nanostructures using graphene. Nano Lett 2013;14:78–82.
[27] Liu S-D, Leong ESP, Li G-C, et al. Polarization-independent multiple Fano resonances in plasmonic nonamers for multimode-matching enhanced multiband second-harmonic generation. ACS Nano 2016;10:1442–53.
[28] Moritake Y, Kanamori Y, Hane K. Demonstration of sharp multiple Fano resonances in optical metamaterials. Opt Express 2016;24:9332–6.
[29] Zhang F, Hu X, Zhu Y, Fu Y, Yang H, Gonga Q. Ultrafast all-optical tunable Fano resonance in nonlinear metamaterials. Appl Phys Lett 2013;102:181109.
[30] Chai Z, Hu X, Gong Q. All-optical switching based on a tunable Fano-like resonance in nonlinear ferroelectric photonic crystals. J Opt 2013;15:085001.
[31] Gu J, Singh R, Liu X, et al. Active control of electromagnetically induced transparency analogue in terahertz metamaterials. Nat Commun 2012;3:1151.
[32] Manjappa M, Srivastava YK, Cong L, Al-Naib I, Singh R. Active photoswitching of sharp Fano resonances in THz metadevices. Adv Mater 2016;29:1603355.
[33] Yan C, Yang KY, Martin OJF. Fano-resonance-assisted metasurface for color routing. Light Sci Appl 2017;6:e17017.
[34] Chen J, Li Z, Li J, Gong Q. Compact and high-resolution plasmonic wavelength demultiplexers based on Fano interference. Opt Express 2011;19:9976–85.
[35] Piggott AY, Lu J, Lagoudakis KG, Petykiewicz J, Babinec TM, Vučković J. Inverse design and demonstration of a compact and broadband on-chip wavelength demultiplexer. Nat Photonics 2015;9:374–7.
[36] Lu C, Liu Y-C, Hu X, Yang H, Gong Q. Integrated ultracompact and broadband wavelength demultiplexer based on multi-component nano-cavities. Sci Rep 2016;6:27428.
[37] Qu C, Ma S, Hao J, et al. Tailor the functionalities of metasurfaces based on a complete phase diagram. Phys Rev Lett 2015;115:235503.

Supplementary Material: The online version of this article offers supplementary material (https://doi.org/10.1515/nanoph-2019-0492).